

---

# Distractor-free Generalizable 3D Gaussian Splatting

---

**Yanqi Bao\***  
 Nanjing University  
 Jiangsu, Nanjing, China  
 yanqibao1997@gmail.com

Jing Liao<sup>†</sup>  
 City University of Hong Kong  
 Hong Kong, China  
 jingliao@cityu.edu.hk

Jing Huo<sup>†</sup>  
 Nanjing University  
 Jiangsu, Nanjing, China  
 huojing@nju.edu.cn

Yang Gao  
 Nanjing University  
 Jiangsu, Nanjing, China  
 gaoy@nju.edu.cn

## Abstract

We present DGGs, a novel framework that addresses the previously unexplored challenge: **Distractor-free Generalizable 3D Gaussian Splatting** (3DGS). It mitigates 3D inconsistency and training instability caused by distractor data in the cross-scenes generalizable train setting while enabling feedforward inference for 3DGS and distractor masks from references in the unseen scenes. To achieve these objectives, DGGs proposes a scene-agnostic reference-based mask prediction and refinement module during the training phase, effectively eliminating the impact of distractor on training stability. Moreover, we combat distractor-induced artifacts and holes at inference time through a novel two-stage inference framework for references scoring and re-selection, complemented by a distractor pruning mechanism that further removes residual distractor 3DGS-primitive influences. Extensive feedforward experiments on the real and our synthetic data show DGGs’s reconstruction capability when dealing with novel distractor scenes. Moreover, our generalizable mask prediction even achieves an accuracy superior to existing scene-specific training methods. Codes and models will be made publicly available.

## 1 Introduction

The widespread availability of mobile devices presents unprecedented opportunities for 3D reconstruction, fostering demand for feedforward 3D synthesis capabilities from casually captured images or video sequences (referred to as references). Recent approaches introduce generalizable 3D representations to address this challenge, eliminating per-scene optimization requirements, with 3D Gaussian Splatting (3DGS) demonstrating particular promise due to its efficiency [2, 16, 5, 31]. In pursuit of scene-agnostic inference from references to 3DGS, existing methods simulate the complete pipeline ‘inputs references infer 3DGS and outputs novel query views’ within each training step, utilizing selected reference-query pairs while optimizing model parameters by query rendering losses.

Following this paradigm, a generalizable 3DGS requires both comprehensive training pairs and a trained scene-independent mechanism to understand 3D geometric correlations between references. However, these essential components face fundamental challenges from the distractor in unconstrained capture scenarios: (1) real-world scenes typically lack distractor-free data for training, and (2) distractor disrupt 3D consistency among limited references during training and inference processes.

To address these problems, a straightforward solution is to integrate scene-specific distractor-free masking methods [3, 27, 24] into training loss of generalizable 3DGS, i.e. ‘MVSplat+’ in Sec. 5.2,

---

\*This work was completed during a visit to City University of Hong Kong.

<sup>†</sup>Corresponding author

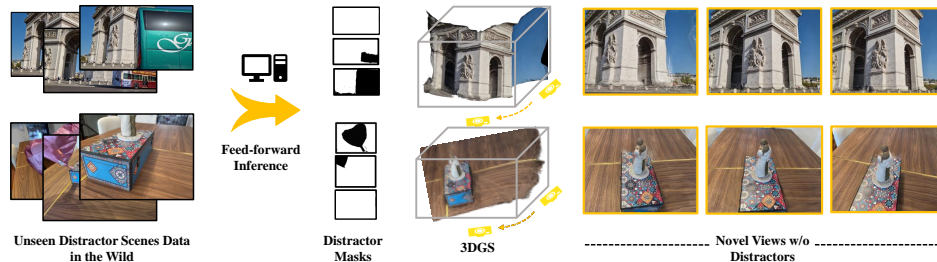


Figure 1: **Overview of Our Task.** *Distractors are unwanted transient objects in static scene reconstruction, such as buses, balloons, or anything.* DGGS enables feedforward 3DGS reconstruction from limited distractor data while inferring corresponding distractor masks without extra supervision.

enabling the prediction of distractor masks from *the outliers of residual loss* and actively suppressing them in loss function that would otherwise compromise training robustness [25]. However, two main limitations emerge in this approach: (1) The existing loss-based masking strategies rely heavily on repeated optimization with sufficient inputs in a single scene and scene-specific hyperparameters [25]. They are ineffective in our cross-scene generalizable training setting, where loss uncertainty increases due to inter-iteration scene transitions and uncertain scene hyperparameters. This uncertainty undermines the core assumption that *high-loss regions correspond to distractor*, potentially misclassifying the part of complex target areas as distractor masks in Fig.3 6 and resulting in inadequate supervision. (2) During feedforward inference, even when accurate masks are obtained, reconstruction in distractor areas continues to be affected by artifacts and remains incomplete due to limited references in Fig.7 8.

For the first challenge, we design a **Distractor-free Generalizable Training paradigm**, incorporating a **Reference-based Mask Prediction** and a **Mask Refinement** module to enhance training stability based on precise generalizable distractor masking. Specifically, inspired by the observation in ‘references to 3DGS’ training paradigm that *re-rendered reference non-distractor areas from 3DGS (inferred by references) are generally accurate and robust*, we use these reference areas as guidance to filter out misclassified distractor regions in query view. This process is realized on the basis of the static geometric multi-view consistency of non-distractor areas. For higher mask accuracy, after decoupling the filtered masks into distractor and disparity error areas, our Mask Refinement module incorporates pre-trained segmentation results to fill distractor regions and a reference-based auxiliary loss to additionally supervise the unnoticed occluded regions in query view.

For the second challenge, which causes holes and artifacts in rendered views, we propose a two-stage **Distractor-free Generalizable Inference framework**. Specifically, in the first stage, we design a **Reference Scoring** mechanism based on the predicted coarse 3DGS and distractor masks from initially sampled references. These predicted scores guide the selection of minimal distractor and disparity references for fine reconstruction in the second stage. To further mitigate ghosting artifacts from residual distractor in the second stage, we introduce a **Distractor Pruning** strategy that eliminates distractor-associated gaussian primitives in the 3D space.

Overall, we address a new task of *Distractor-free Generalizable 3DGS* as in Fig. 1, and this is, to our knowledge, the first work to explore this problem. For this objective, we present **DGGS**, a framework designed to alleviate distractor-related adverse effects during the training and inference phases of generalizable 3DGS. Extensive feedforward experiments on real distractor data have shown that our approach successfully enhances training robustness and improves artifacts and holes during inference while expanding cross-scene (outdoor scenes training and indoor scenes inference) generalizability in conventional scene-specific distractor-free models [3, 25, 23, 24]. Beyond real data, we also construct some synthetic distractor scenes based on Re10K and ACID datasets for further verification. Furthermore, our reference-based training paradigm achieves better generalizable distractor masking *without any mask supervision*, even outperforming scene-specific training distractor-free works[3].

## 2 Related Works

### 2.1 Generalizable 3D Reconstruction

Contemporary advances in generalizable 3D reconstruction seek to establish scene-agnostic representations, building upon early explorations in Neural Radiance Fields [19, 29, 28, 17, 1]. However,

these methods face significant bottlenecks due to their lack of explicit representations and rendering inefficiencies. The advent of 3D Gaussian Splatting [8], an explicit representation optimized for efficient rendering, has sparked renewed interest in the field. Existing works involve inferring Gaussian primitive attributes from references directly and rendering in novel views. Analogous to NeRF-based approaches, 3DGS-related methods emphasize spatial comprehension from references, particularly focusing on depth estimation [2, 5, 16, 31, 12]. Subsequently, ReconX [15] and G3R [6] enhance reconstruction quality through the integration of additional video diffusion models and supplementary sensor inputs. The inherent reliance on high-quality references, however, makes generalizable reconstruction particularly susceptible to **distractor**, a persistent challenge in real-world applications. In this study, we discuss Distractor-free Generalizable 3DGS, an unexplored topic in the current works.

## 2.2 Scene-specific Distractor-free Reconstruction

It focuses on accurately reconstructing a *specific* static scene while mitigating the impact of distractor [23] (or transient objects [25]). As a pioneering work, NeRF-W [18] introduces additional embeddings to represent and eliminate transient objects in unstructured photo collections. Following a similar setting, subsequent works focus on mitigating the impact of distractor *at the image level*, which can generally be categorized into knowledge-based and heuristics-based methods.

**Knowledge-based methods** predict distractor using external knowledge sources. Among them, pre-trained features from ResNet [32, 30], diffusion models [24], and DINO [23, 10] guide visibility map prediction, effectively weighting reconstruction loss. Recent works [3, 21, 20] directly employ state-of-the-art segmentation models such as SAM [9] or Entity Segmentation [22] to establish clear distractor boundaries. Although these approaches demonstrate certain improvements [18, 4, 11] with additional priors, they struggle to differentiate the distractor from static target scenes [3, 21].

**Heuristics-based approaches** employ handcrafted statistical metrics to distinguish distractor, emphasizing robustness and uncertainty analysis [25, 7, 27]. These methods exploit the observation that regions containing distractor typically manifest optimization inconsistencies. Therefore, they seek to predict outliers and mitigate their impact in residual losses. Regrettably, these approaches suffer from significant scene-specific data dependencies and frequently confound distractor with inherently challenging reconstruction regions, limiting their effectiveness in generalizable contexts.

Recently, there has been increasing advocacy for integrating the two methods mentioned above [21, 3]. Entity-NeRF [21] integrates an existing Entity Segmentation [22] and extra entity classifier to determine distractor among entities by analyzing the rank of residual loss. Similarly, NeRF-HuGS [3] integrates pre-defined Colmap and Nerfacto [26] for capturing high and low-frequency features of static targets, while using SAM [9] to predict clear distractor masks. However, in our settings, acquiring additional entity classifiers or employing pre-defined scene-level knowledge such as Colmap and Nerfacto is nearly impossible, and residual loss becomes unreliable compared to single-scene optimization due to the absence of iteratively refined representation. Moreover, with limited references in unseen scenes, despite obtaining distractor masks, traditional Distractor-free methods struggle to handle occluded regions and artifacts. Therefore, we present a novel **Distractor-free Generalizable** framework that jointly addresses distractor effects in training and inference phases.

## 3 Preliminaries

### 3.1 3D Gaussian Splatting

3DGS  $\mathcal{G}$  represents 3D scenes by splatting numerous anisotropic gaussian primitives. Each gaussian primitive is characterized by a set of attributes  $\mathbb{A}$ , including position  $\mathbf{p}$ , opacity  $\alpha$ , covariance matrix  $\Sigma$ , and spherical harmonic coefficients for color  $\hat{\mathbf{c}}$ . To ensure positive semi-definiteness, the covariance matrix  $\Sigma$  is decomposed into a scaling matrix  $\mathbf{S}$  and a rotation matrix  $\mathbf{R}$ , such that  $\Sigma = \mathbf{R}\mathbf{S}\mathbf{S}^\top\mathbf{R}^\top$ . Consequently, the color value after splatting on view  $\mathbf{P}$  is:

$$\hat{\mathbf{C}} = \mathcal{G}(\mathbf{P}) = \sum_{m \in M} \hat{\mathbf{c}}_m \alpha_m \prod_{j=1}^{m-1} (1 - \alpha_j), \quad (1)$$

where  $\hat{\mathbf{c}}_m$  and  $\alpha_m$  are derived from the covariance matrix  $\Sigma_m$  of the  $m$ -th projected 2D Gaussian, as well as the corresponding spherical harmonic coefficients and opacity, respectively.

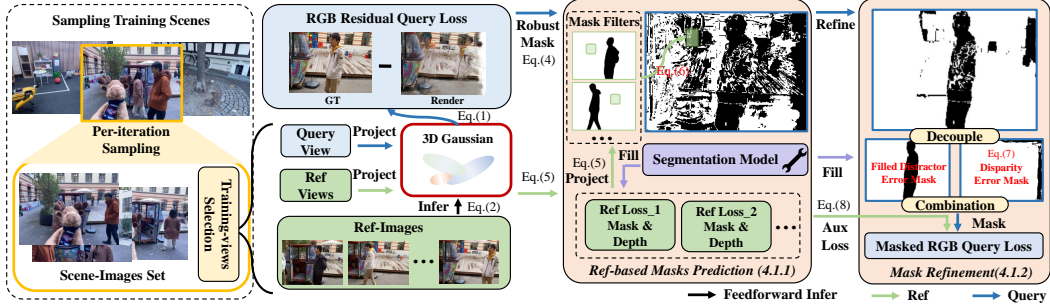


Figure 2: **Distractor-free Generalizable Training.** Based on the sampled reference-query pairs, DGGS first predicts 3DGS attributes and a fundamental robust mask  $\mathcal{M}_{Rob}$ . The **Reference-based Mask Prediction** module then filters this mask, which is further refined through the **Mask Refinement** module. The entire process is supervised through masked query loss and auxiliary loss.

### 3.2 Generalizable 3DGS

Generalizable 3DGS presents a novel paradigm that directly infers 3DGS  $\mathcal{G}$  attributes from references, circumventing the computational overhead of scene-specific optimization. During each training iteration, existing works optimize model parameters  $\theta$  by randomly sampling paired references  $\{\mathbf{I}_i\}_{i=1}^N$  and query image  $\mathbf{I}_T$  as inputs and groundtruth under random sampled scenes. Specifically,

$$\mathcal{G} = \text{Decoder} \left( \mathcal{F} \left( \text{Encoder} \left( \{\mathbf{I}_i\}_{i=1}^N, \{\mathbf{P}_i\}_{i=1}^N \right) \right) \right), \quad \arg \min_{\theta} \|\mathbf{I}_T - \mathcal{G}(\mathbf{P}_T)\|_2^2, \quad (2)$$

where  $\{\mathbf{P}_i\}_{i=1}^N$  and  $\mathbf{P}_T$  are the camera extrinsics of the reference and query images, and  $N$  denotes the number of references. The  $\mathcal{F}$  denotes the process of projecting encoded 2D features into 3D space and refining [5, 2]. The 3D features are then decoded into the corresponding 3DGS attributes and rendered into query views, through which the network can be optimized by the query MSE loss.

### 3.3 Robust Masks for 3D Reconstruction

Unlike conventional controlled static environments, our in-the-wild scenarios contain not only static elements but also distractor [25], making it difficult to maintain 3D geometric consistency and training stability. Building on prior Scene-specific Distractor-free reconstruction research [25, 24, 23, 3], we integrate the mask-based robust optimization loss in our pipeline (i.e. ‘MVSplat+ \*’ in experiment, where \* represents different mask prediction methods) that can predict and filter out distractor (outliers) in training process. Hence, Eq. 2 is modified, where  $\odot$  denotes pixel-wise multiplication:

$$\arg \min_{\theta} \mathcal{M}_{Rob} \odot \|\mathbf{I}_T - \mathcal{G}(\mathbf{P}_T)\|_2^2. \quad (3)$$

Here,  $\mathcal{M}_{Rob}$  represents the outlier masks on query view, where distractor is set to zero, while target static regions are set to one. Our work introduces a simple heuristic method [25] as the foundation. The hyperparameters  $\rho_1$  and  $\rho_2$  are fixed across all scenes.

$$\mathcal{M}_{Rob} = \mathbb{1} \{ \mathcal{C} (\mathbb{1} \{ \|\mathbf{I}_T - \mathcal{G}(\mathbf{P}_T)\|_2 < \rho_1 \}) > \rho_2 \}, \quad (4)$$

where  $\mathcal{C}$  represents the kernel operator and the  $\rho_1$  as well as  $\rho_2$  remain consistent with [25]. Despite various mask refinements in follow-up studies [21, 3, 24], their heavy dependence on loss  $\|\mathbf{I}_T - \mathcal{G}(\mathbf{P}_T)\|_2$  leads to extensive misclassification of difficult-to-feedforward-inference parts as distractor regions, as show in Fig. 3 and Fig. 6, which is addressed in subsequent sections.

## 4 Method

Given sufficient training reference-query pairs, the presence of distractor in either  $\{\mathbf{I}_i\}_{i=1}^N$  or  $\mathbf{I}_T$  (or both) affects the 3D consistency relied upon by generalizable models. Therefore, we aim to design a **Distractor-free Generalizable Training** paradigm in Sec. 4.1 and a Inference framework in Sec. 4.2.



Figure 3: **The Mask Evolution in Sec. 4.1.**  $\mathcal{M}_Q$  is obtained by filtering  $\mathcal{M}_{Rob}$  from the references non-distractor regions, which is then filled by decoupling  $\mathcal{M}_D$  and using segmentation results to get final  $\mathcal{M}$  as Eq. 4 6 7 8. Without references filter, target regions are often misidentified as distractor.

#### 4.1 Distractor-free Generalizable Training

In this training paradigm, we propose a **Reference-based Mask Prediction** in Sec.4.1.1 and a **Mask Refinement** module in Sec.4.1.2 to enhance per-iteration distractor mask prediction accuracy and training stability scene-agnostically in generalizable setting, as illustrated in Fig. 2.

##### 4.1.1 Reference-based Mask Prediction

This Mask Prediction module aims to enhance the  $\mathcal{M}_{Rob}$  accuracy within each iterative various scene, ensuring that optimization efforts remain focused on more non-distractor areas. It is essential for generalization training, since Eq. 4 inevitably misclassifies certain target regions as distractor, particularly those presenting challenges for feedforward inference, as in Fig. 3 6, which impedes the model’s comprehension of geometric 3D consistency in Fig. 5. Our inspiration stems from an intuitive observation: *the 3DGS inferred from references maintains stable and accurate re-rendering results in non-distractor regions under reference views*. Specifically, we introduce a mask **filter** that harnesses non-distractor regions from re-rendered references (i.e. from references to infer 3DGS and render back to reference views) to identify and remove falsely labeled distractor regions in  $\mathcal{M}_{Rob}$  under query view, based on the multi-view consistency of non-distractor static objects. Given  $i \in N$  denotes references and  $\rho_{Ref}$  is a hyperparameter (as 0.001), discussed in Fig. 9, re-rendered reference non-distractor masks  $\mathcal{M}_{Ref_i}$  and corresponding projected query masks  $\mathcal{M}_{Qry_i}$  are

$$\mathcal{M}_{Ref_i} = \mathbb{1} \left\{ \|\mathbf{I}_i - \mathcal{G}(\mathbf{P}_i)\|_2^2 < \rho_{Ref} \right\}, \quad \mathcal{M}_{Qry_i} = \mathcal{W}_{i \rightarrow T}(\mathcal{M}_{Ref_i}, \mathbf{D}_i, \mathbf{P}_i, \mathbf{P}_T, \mathbf{U}), \quad (5)$$

where  $\mathbf{U}$  represents the camera intrinsic matrix of image pairs,  $\mathbf{D}_i$  corresponds to the depth maps rendered from  $\mathbf{P}_i$  utilizing a modified rasterization library,  $\mathcal{W}_{i \rightarrow T}$  defines the image warping that projects each  $\mathcal{M}_{Ref_i}$  from  $\mathbf{P}_i$  to  $\mathbf{P}_T$  using  $\mathbf{D}_i$  and  $\mathbf{U}$ .

However, given the inherent noise presence in  $\mathcal{M}_{Ref_i}$ ,  $\mathcal{M}_{Qry_i}$  exhibits limited precision. To solve this problem, we incorporate a pre-trained segmentation model for mask filling, while designing a multi-mask fusion strategy to counteract noise-induced deviations. Following [3, 21], we incorporate a state-of-the-art Entity Segmentation Model [22] to refine  $\mathcal{M}_{Ref_i}$  into  $\mathcal{M}_{Ref_i}^{En}$ , which has the capability to fill different entities when the predicted distractor-region exceeds the threshold of total pixel count for that entity. After substituting  $\mathcal{M}_{Ref_i}$  with  $\mathcal{M}_{Ref_i}^{En}$  in Eq. 5, we use an intersection operation to fuse all ( $N$ )  $\mathcal{M}_{Qry_i}$ , then filter  $\mathcal{M}_{Rob}$  based on it, obtaining the reference-based mask  $\mathcal{M}_Q$ , which can filter out misclassified regions in  $\mathcal{M}_{Rob}$  to some extent, as shown in Fig. 3.

$$\mathcal{M}_Q = \left\{ \bigcap_{i=1}^N \mathcal{M}_{Qry_i} \right\} \cup \mathcal{M}_{Rob}. \quad (6)$$

Here, we employ the intersection as a conservative strategy to ensure that the filtered-out regions in  $\mathcal{M}_{Rob}$  are non-distractor regions acknowledged by all references and preserve the potential distractor are excluded from optimization regions, which is crucial for the training process. However,  $\mathcal{M}_Q$  still exhibits limitations in accurate distractor masking, due to incorrect  $\mathbf{D}_i$  prediction and view disparities, as illustrated in Fig. 3. Consequently, the distractor masks undergo further refinement in Sec. 4.1.2.

##### 4.1.2 Mask Refinement

Given  $\mathcal{M}_Q$ , a straightforward approach is to utilize a pre-trained segmentation model to refine noise regions and fill imprecise warping areas, as discussed with respect to  $\mathcal{M}_{Ref_i}^{En}$ . In contrast to

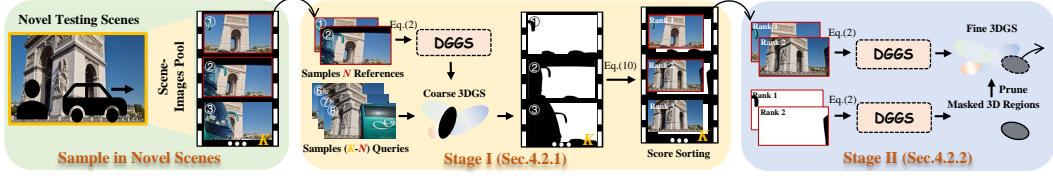


Figure 4: **Distractor-free Generalizable Inference Framework.** DGGs initially samples adjacent references from the scene-images pool and leverages trained DGGs for coarse 3DGS. Based on the **Reference Scoring mechanism**, masks and quality scores are computed for all pool images. These masks and scores subsequently guide reference selection and **Distractor Pruning** for fine 3DGS.

references,  $\mathcal{M}_Q$  contains distractor regions and disparity-induced errors arising from reference-query view variations, simultaneously, the latter being present in the query view but absent in all references and primarily occurring at the query image margins. Thus, before introducing the segmentation model, regions decoupling is essential, where the prediction of the disparity-induced error mask can follow a deterministic approach. Given  $N$  one-filled masks  $\mathcal{M}_i^1$  corresponding to different reference views  $\mathbf{P}_i$ , we warp them to the target view  $\mathbf{P}_T$  as in Eq. 5. Then, the warped masks are merged using a union operation to ensure that these regions are absent from all references as Fig. 3.

$$\mathcal{M}_D = \bigcup_{i=1}^N \{ \mathcal{W}_{i \rightarrow T} (\mathcal{M}_i^1, \mathbf{D}_i, \mathbf{P}_i, \mathbf{P}_T, \mathbf{U}) \}. \quad (7)$$

Finally, we decouple  $\mathcal{M}_D$  from  $\mathcal{M}_Q$  and recombine them after introducing the segmentation model [22] and refining the distractor mask. The final refined mask, termed  $\mathcal{M}$  in Fig. 3, substitutes  $\mathcal{M}_{Rob}$  in Eq. 3 to mitigate distractor effects during training. Furthermore, we observe that if only Mask Refinement is used, without leveraging reference and our observation, the misclassification remains severe in Fig. 3, which verifies the importance of our reference filter in Sec. 4.1.1.

Additionally, in contrast to traditional distractor-free frameworks, references enable auxiliary supervision in the query view, providing guidance for occluded areas. Specifically, we re-warp  $\mathcal{M}$  to reference views and utilize  $\mathcal{M}_{Ref_i}^{En}$  to determine whether occlusion information is included. Therefore, our auxiliary loss  $\mathcal{L}_A$  can focus on areas occluded from query view but visible from references.

$$\mathcal{L}_A = \sum_N^{i=1} \mathcal{W}_{T \rightarrow i} (1 - \mathcal{M}) \odot \mathcal{M}_{Ref_i}^{En} \odot \|\mathbf{I}_i - \mathcal{G}(\mathbf{P}_i)\|_2^2. \quad (8)$$

All pre-trained segmentation are pre-computed and cached. The final form of Eq. 3 is modified to:

$$\arg \min_{\theta} \mathcal{M} \odot \|\mathbf{I}_T - \mathcal{G}(\mathbf{P}_T)\|_2^2 + \mathcal{L}_A. \quad (9)$$

## 4.2 Distractor-free Generalizable Inference

Despite improvements in training robustness and mask prediction, DGGs’s inference faces two key limitations: (1) insufficient references compromise reliable reconstruction of occluded and unseen regions; (2) persistent distractor in references inevitably appear as artifacts in synthesized novel views for feedforward inference paradigm (encoder-decoder) in Eq. 2. To address these challenges, we propose a two-stage **Distractor-free Generalizable Inference** framework in Fig. 4. The first stage employs a **Reference Scoring** mechanism in Sec.4.2.1 to score candidate references from the images pool, facilitating the selected references with minimal distractor and disparity. The second stage uses a **Distractor Pruning** module in Sec.4.2.2 to suppress the remaining artifacts.

### 4.2.1 Reference Scoring Mechanism

The objective of the first inference stage is to select references with minimal distractor and disparity among the predefined scene-images pool, adjacent  $K$  views ( $K \geq N$ ) sampled in the test scenes. Therefore, we propose a Reference Scoring mechanism based on the pre-trained DGGs in Sec. 4.1. Specifically, it first samples  $N$  adjacent references near the query from the scene-images pool  $\{\mathbf{I}\}_P^K$  for coarse 3DGS prediction. We then designate unselected views from  $\{\mathbf{I}\}_P^K$  as query for mask

Table 1: **Quantitative Experiments for distractor-free Generalizable 3DGS** under RobustNeRF. \* denotes pre-trained models, + indicates baseline models augmented with existing masking methods.

Methods	Statue (RobustNeRF)			Android (RobustNeRF)			Mean (Five Scenes)			Train Data
	PSNR↑	SSIM↑	LPIPS↓	PSNR↑	SSIM↑	LPIPS↓	PSNR↑	SSIM↑	LPIPS↓	
PixelSplat* (2024 CVPR) [2]	18.65	0.673	0.254	17.98	0.557	0.364	20.10	0.704	0.279	Pre-Train on Re10K
Mvsplat* (2024 ECCV) [5]	18.88	0.670	<b>0.225</b>	18.24	0.586	0.301	20.03	0.722	0.255	
PixelSplat (2024 CVPR) [2]	15.49	0.378	0.531	16.34	0.331	0.492	16.02	0.422	0.511	Re-Train on Distractor-Datasets
Mvsplat (2024 ECCV) [5]	15.05	0.412	0.391	16.17	0.509	0.381	15.45	0.515	0.426	
+RobustNeRF (2023 CVPR) [25]	16.17	0.463	0.382	16.46	0.470	0.411	17.11	0.534	0.400	
+On-the-go (2024 CVPR) [23]	14.73	0.366	0.522	15.05	0.440	0.472	15.44	0.476	0.526	
+NeRF-HuGS (2024 CVPR) [3]	18.21	0.694	0.266	18.33	0.640	0.299	19.18	0.700	0.283	
+SLS (Arxiv 2024) [24]	18.11	0.695	0.270	18.84	<b>0.662</b>	0.282	19.29	0.709	0.286	
DGGS-TR (w/o Inference Part)	<b>19.68</b>	<b>0.700</b>	0.238	<b>19.58</b>	0.653	<b>0.286</b>	<b>21.02</b>	<b>0.738</b>	<b>0.242</b>	
DGGS (Our)	<b>20.78</b>	<b>0.710</b>	<b>0.233</b>	<b>20.93</b>	<b>0.711</b>	<b>0.236</b>	<b>21.74</b>	<b>0.758</b>	<b>0.237</b>	

Table 2: **Ablation** for DGGS-TR and DGGS.

Methods	Mean (Five Scenes)		
	PSNR↑	SSIM↑	LPIPS↓
<b>Ablation on Our Training Paradigm</b>			
Baseline (Mvsplat)	15.45	0.515	0.426
+Robust Mask	17.11	0.534	0.400
++Ref-based Mask Prediction	20.35	0.701	0.283
+++Mask Refinement (DGGS-TR)	<b>21.02</b>	<b>0.738</b>	<b>0.242</b>
w/o Reference Entity Segmentation	20.79	0.733	0.248
w/o Aux Loss	20.64	0.725	0.253
<b>Ablation on Our Inference Framework</b>			
DGGS-TR	21.02	0.738	0.242
+ Reference Scoring mechanism	21.47	0.749	0.242
++ Distractor Pruning (DGGS)	<b>21.74</b>	<b>0.758</b>	<b>0.237</b>

Table 3: **Comparison** of Fine-Tuned models.

Methods	Arcdetriomphe			Mountain		
	PSNR↑	SSIM↑	LPIPS↓	PSNR↑	SSIM↑	LPIPS↓
Mvsplat*+FT	23.58	0.841	0.08	17.06	0.622	0.202
Mvsplat*+SLS-FT	27.19	0.916	0.084	22.03	0.698	0.160
Mvsplat*+DGGS-FT	28.61	0.922	0.068	23.00	0.723	0.144
(Mvsplat+SLS)*+SLS-FT	24.18	0.887	0.095	20.77	0.645	0.189
DGGS-TR*+DGGS-FT	<b>29.04</b>	<b>0.931</b>	<b>0.058</b>	<b>23.85</b>	<b>0.787</b>	<b>0.128</b>

Table 4: **Ablations** for Reference Scoring.

Methods	Mean (RobustNeRF)		
	PSNR↑	SSIM↑	LPIPS↓
DGGS-TR (N=4)	21.02	0.738	0.242
DGGS-TR (N=8)	20.22	0.690	0.311
DGGS w/o Pruning (N=4)	<b>21.47</b>	<b>0.749</b>	<b>0.242</b>

Table 5: **Comparison** on Efficiency.

Methods	PixelSplat	Mvsplat	DGGS (Two Stage Inference)
Rendering Time (s)	0.160	<b>0.084</b>	0.148 [w pre-segmentation 0.111]

prediction  $\{\mathcal{M}\}^{K-N}$ , while the distractor masks of the chosen reference views are  $\{\mathcal{M}_{Ref}^{En}\}^N$ . All image masks in pool are scored by Eq. 10, in which top  $N$  images are selected in next stage,

$$\{\mathbf{I}_i\}^N = \{\mathbf{I}_i\}_P^K \mid i \in \arg \max_N \{\mathcal{S}(\{\mathcal{M}\}^{K-N}; \{\mathcal{M}_{Ref}^{En}\}^N)\}. \quad (10)$$

where  $\mathcal{S}$  is the pixel-wise summation for each mask. In practice, besides distractor size, the extrinsics of candidate images are also crucial reference scoring factors due to disparity. Thanks to the discussion of disparity-induced error masks in Sec. 4.1.2, we can directly utilize the count of positive pixels in  $\mathcal{M}$  as the single criterion, which selects references that provide better coverage of query view, as shown in Fig. 7 8. In the second stage, we employ top-ranked images as references for fine reconstruction, effectively reselecting the candidate images in the pool without increasing GPU memory. Although this approach successfully handles distractor-heavy references, it comes at the cost of decreased rendering efficiency. Optionally, we mitigate this by halving the image resolution in the first stage.

## 4.2.2 Distractor Pruning

Although cleaner references are selected, obtaining  $N$  distractor-free images in the wild is virtually impossible. These residual distractor propagate via the gaussian encoding-decoding process in Eq. 2, manifesting as phantom splats in rendered query view, as shown in Fig. 8. Therefore, we propose a Distractor Pruning protocol in the second inference stage, which is readily implementable given the reference distractor masks in Sec. 4.2.1. Instead of direct masking on the references, which affects one-to-one mapping between pixels and gaussian primitives in Eq. 2, we selectively prune gaussian primitives within the 3D space by directly removing decoded attributes in distractor regions while preserving the remaining components. However, when references exhibit a large amount of commonly occluded regions, the pruning strategy induces white speckle artifacts. Consequently, based on projected masks, DGGS implements the pruning strategy only in scenarios where it is not considered a common occluded region for all references, which is also discussed in Limitation.

## 5 Experiments

This section presents qualitative and quantitative results for DGGS in real-world and our synthetic generalization scenarios with distractor, which validate the reliability of our training and inference paradigm. Also, multi-scene experiments show that DGGS enables existing distractor-free methods to generalize in reconstruction and masking, overcoming their lack of cross-scene inference.

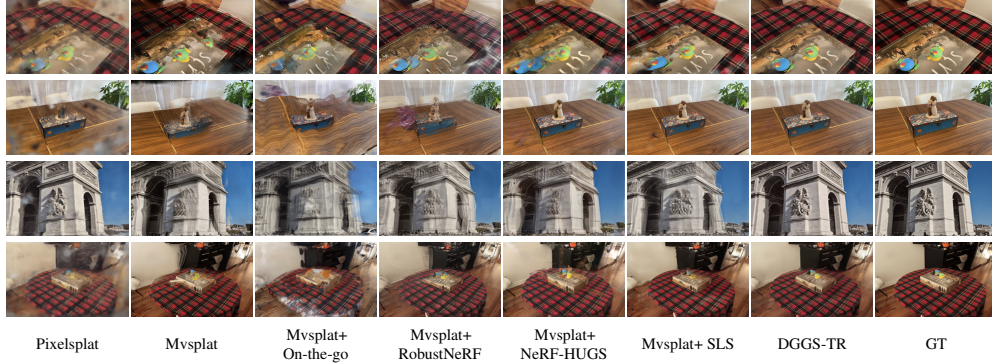


Figure 5: **Qualitative Comparison of Re-trained Existing Methods** across unseen scenes.



Figure 6: **Qualitative Comparison** for our masks prediction vs. scene-specific results.

## 5.1 Experimental Details

### 5.1.1 Real and Synthetic Distractor Datasets

In accordance with existing generalization frameworks, DGGs is trained in a cross-scene setting with distractor and evaluated in novel unseen distractor scenes to simulate real-world scenarios. Specifically, we utilize two widely used mobile-captured datasets: On-the-go [23] and RobustNeRF [25], containing multiple distractor-scenes in outdoor and indoor environments, respectively. For fair comparison in real data, we train all models on On-the-go outdoor-scenes except *Arcdetriomphe* and *Mountain*, which, along with the RobustNeRF indoor-scenes, serve as test scenes. In addition to real data, we also construct synthetic datasets for additional verification. Specifically, we randomly insert distractor from COCO [13] into Re10K [33] and ACID [14] data, with details described in Appendix.

### 5.1.2 Training and Evaluation Setting

In all experiments, we set the number of references  $N=4$  and the size of scene-images pool  $K=8$ , which are discussed in Fig. 9. During all training, query views are randomly selected and reference views are chosen following the nearest-neighbor selection strategy, regardless of ‘clutter’ or ‘extra’. In evaluation phase, we utilize all ‘extra’ images and ‘clear’ images with a stride of eight as query views for On-the-go (*Arcdetriomphe* and *Mountain*) and all RobustNeRF scenes. For references in evaluation, we construct the scene-images pool using views closest to the query view, ensuring inclusion of both distractor-containing and few distractor-free data to validate the effectiveness of Reference Scoring mechanism. Note that this setting is only for validation and evaluation purposes. In practical applications, the scene-images pool can be constructed using any adjacent views, independent of the query view and distractor presence. Finally, we compute the average PSNR, SSIM, and LPIPS metrics across all scenes on all query renders. More details are described in Appendix.



Figure 7: **Qualitative Comparison of Pre-trained Models, DGGS-TR and DGGS.**

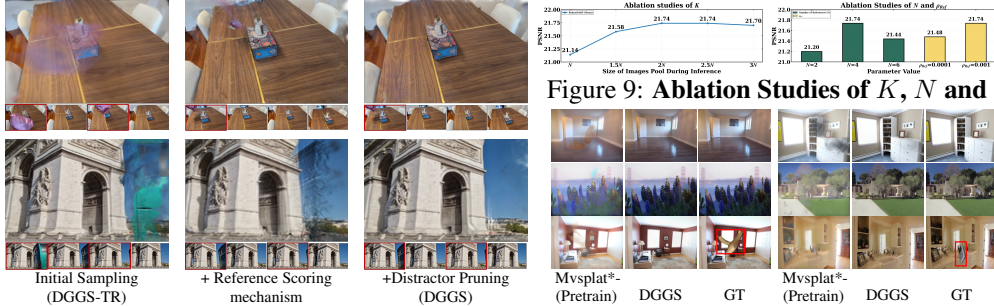


Figure 9: **Ablation Studies of  $K$ ,  $N$  and  $\rho_{Ref}$ .**

Figure 8: **Ablation for Inference Strategy.**

Figure 10: **Comparison on synthetic data.**

## 5.2 Comparative Experiments

### 5.2.1 Benchmark

Our Distractor-free Generalizable training and inference paradigms can be seamlessly integrated with existing generalizable 3DGS frameworks. We adopt Mvsplat [5] as our baseline model. Extensive comparisons are conducted against existing works trained under same settings and distractor datasets, including: **(1) retraining** existing generalization methods [5, 2], and **(2) retraining** Mvsplat [5] ‘+’ different mask prediction strategies from distractor-free approaches [23, 25, 3, 24]. Although all current distractor-free works are scene-specific, most of them focus on applying distractor masks in loss function (as discussed in Sec. 2.2), so we can directly transfer them to the query rendering loss under our baseline. Specifically, during the training phase, we combine these mask prediction methods from existing works and replace  $\mathcal{M}_{Rob}$  in Eq. 3. Furthermore, **(3)** we compare with existing **pre-trained** generalizable models (on distractor-free data). More details are provided in Appendix.

### 5.2.2 Quantitative and Qualitative Experiments

Tab. 1, Fig. 5 and Fig. 7 quantitatively and qualitatively compares DGGS-TR (only TRaining in Sec. 4.1 without two stages inference in Sec. 4.2) and DGGS with existing methods. The results are analyzed from three aspects: re-training models, pre-training models and models after fine-tuning.

**For Re-train Model:** Tab. 1 and Fig. 5 demonstrate that our training paradigm significantly enhances training robustness, outperforming existing generalizable 3DGS algorithms, **PSNR: 21.02 vs. 15.45**, under same training conditions. Compared to introducing existing scene-specific distractor-free approaches, where overaggressive distractor prediction degrades reconstruction fidelity, DGGS-TR exhibits enhanced reconstruction detail and 3D consistency, **PSNR: 21.02 vs. 19.29**, through precise distractor prediction, which is further validated in Fig. 6. Similarly, the qualitative results in Fig. 5 show training instability and significant performance drops, even without distractors in some test references. It confirms that distractor presence severely impairs model learning of geometric 3D consistency, aligning with our motivation. Additionally, experiments also show that DGGS possesses cross-scene feedforward inference capabilities that existing distractor-free methods lack.

**For Pre-train Model:** Tab. 1 reports comparisons between DGGS-TR, DGGS and existing pre-train generalizable models. Compared with pre-train models on distractor-free data, DGGS-TR exhibits superior performance even with training on limited distractor scenes, mainly due to mitigating the inference scene *distractor impacts* and *domain gap*. Fig. 7 also illustrates similar findings: DGGS-TR

effectively attenuates partial distractor effects in the 3D inconsistency regions. Furthermore, after introducing our inference paradigm, DGGs demonstrates ‘pseudo-completion’ and artifact removal capabilities, which benefit from the **Reference Selection** mechanism that can choose references with less distractor as well as disparity and the **Distractor Pruning** during inference process as in Fig. 8. To further validate effectiveness, we compare DGGs’s results on synthetic data, which maintains the same data domain as the pre-trained MVSplat\* except for inserted distractor. In Fig. 10, DGGs shows better resistance to distractor, effectively mitigating artifact. More results are shown in Appendix.

**After Fine-tuning:** To further demonstrate DGGs’s capability, we conduct fine-tuning experiments on the different pre-trained models (including Mvsplat\*, (Mvsplat+SLS)\* and DGGs-TR\* corresponding Line 2, 8, and 9 in Tab. 1) and training strategies (including FT, SLS-FT and DGGs-FT corresponding Mvsplat [5], SLS [24] and Ours). We fine-tune using the ‘clutter’ data and evaluate on the ‘extra’ data in test scenes. For fairness in comparison, our inference framework is not employed. In Tab. 3, DGGs-TR demonstrates significant improvements over existing models and strategies, attributed to our reliable distractor prediction. More qualitative results are shown in Appendix.

**Efficiency:** Tab. 5 shows the efficiency comparison. Due to the segmentation model and two-stage inference, DGGs has a slight decrease in efficiency compared to [5], but mitigates distractor and obtains masks. It can be boosted by reducing segmentation resolution or lighter segmentation models.

### 5.3 Ablation Studies

#### 5.3.1 Ablation on Training Framework

The upper section of Tab. 2 and Fig. 3 show the effectiveness of each component in DGGs training paradigm. The Reference-based Mask Prediction combined with Mask Refinement successfully mitigates the tendency of over-predicting targets as distractor that occurred in the original  $\mathcal{M}_{Rob}$ . Within the Mask Refinement module, Auxiliary Loss demonstrates remarkable performance, while Mask Decoupling and Entity Segmentation contribute substantial improvements to the overall framework. Furthermore, our analysis in Fig. 6 reveals that DGGs-TR achieves scene-agnostic mask prediction capabilities, with feedforward inference results superior to single-scene trained models [3]. Note that, for fair evaluation, all masks are predicted under DGGs-TR based same references, without the involvement of our inference framework.

#### 5.3.2 Ablation on Inference Framework

The bottom portion of Tab. 2, Fig. 7, and Fig. 8 analyze the component effectiveness within the inference paradigm. Results indicate that although the Reference Scoring mechanism alleviates the impact of distractor in references by re-selection, red box represent distractor references in Fig. 8, certain artifacts remain unavoidable. Then, our Distractor Pruning strategy effectively mitigates these residual artifacts. We also analyze how the choice of  $K$  and  $N$  in DGGs, the sizes of scene images pool and references, affects inference results in Fig. 9. Generally, larger values of  $K$  yield better performance up to  $2N$ , beyond which performance plateaus, likely due to increased significant view disparity in the images pool. A similar situation occurs with  $N$ , where excessive references actually increase distractor and disparity. And, Tab. 4 explores why the Reference Scoring mechanism brings performance improvements. A potential possibility is our ability to access more references during inference [5]. Therefore, we directly select more references in DGGs-TR using the nearest neighbor strategy. Experimental findings indicate, incorporating additional references directly will introduce novel artifacts. It proves that the quality of references takes precedence over quantity in our setting, and the proposed Reference Scoring mechanism can filter out higher-quality references.

## 6 Conclusion

Distractor-free Generalizable 3D Gaussian Splatting presents a practical challenge, offering the potential to mitigate the limitations imposed by distractor scenes on generalizable 3DGS while addressing the scene-specific training constraints of existing distractor-free methods. We propose novel training and inference paradigms that alleviate both training instability and inference artifacts from distractor data. Extensive experiments across diverse scenes validate our method’s effectiveness and demonstrate the potential of the reference-based paradigm in handling distractor scenes. We envision

this work laying the foundation for future community discussions on Distractor-free Generalizable 3DGS and potentially extending to address real-world 3D data challenges in broader applications.

**Limitation:** DGGs mitigates distractors but experiences performance degradation under extensive common occlusions. Generative models offer a potential solution. In addition, the sacrifice in efficiency is unavoidable, which can be mitigated through lighter segmentation models and resolution.

## References

- [1] Yanqi Bao, Tianyu Ding, Jing Huo, Wenbin Li, Yuxin Li, and Yang Gao. Insertnerf: Instilling generalizability into nerf with hypernet modules. *arXiv preprint arXiv:2308.13897*, 2023.
- [2] David Charatan, Sizhe Lester Li, Andrea Tagliasacchi, and Vincent Sitzmann. pixelsplat: 3d gaussian splats from image pairs for scalable generalizable 3d reconstruction. In *Proceedings of the IEEE/CVF Conference on Computer Vision and Pattern Recognition*, pages 19457–19467, 2024.
- [3] Jiahao Chen, Yipeng Qin, Lingjie Liu, Jiangbo Lu, and Guanbin Li. Nerf-hugs: Improved neural radiance fields in non-static scenes using heuristics-guided segmentation. In *Proceedings of the IEEE/CVF Conference on Computer Vision and Pattern Recognition*, pages 19436–19446, 2024.
- [4] Xingyu Chen, Qi Zhang, Xiaoyu Li, Yue Chen, Ying Feng, Xuan Wang, and Jue Wang. Hallucinated neural radiance fields in the wild. In *Proceedings of the IEEE/CVF Conference on Computer Vision and Pattern Recognition*, pages 12943–12952, 2022.
- [5] Yuedong Chen, Haofei Xu, Chuanxia Zheng, Bohan Zhuang, Marc Pollefeys, Andreas Geiger, Tat-Jen Cham, and Jianfei Cai. Mvsplat: Efficient 3d gaussian splatting from sparse multi-view images. *arXiv preprint arXiv:2403.14627*, 2024.
- [6] Yun Chen, Jingkang Wang, Ze Yang, Sivabalan Manivasagam, and Raquel Urtasun. G3r: Gradient guided generalizable reconstruction. In *European Conference on Computer Vision*, pages 305–323. Springer, 2025.
- [7] Lily Goli, Cody Reading, Silvia Sellán, Alec Jacobson, and Andrea Tagliasacchi. Bayes’ rays: Uncertainty quantification for neural radiance fields. In *Proceedings of the IEEE/CVF Conference on Computer Vision and Pattern Recognition*, pages 20061–20070, 2024.
- [8] Bernhard Kerbl, Georgios Kopanas, Thomas Leimkühler, and George Drettakis. 3d gaussian splatting for real-time radiance field rendering. *ACM Transactions on Graphics*, 42(4):1–14, 2023.
- [9] Alexander Kirillov, Eric Mintun, Nikhila Ravi, Hanzi Mao, Chloe Rolland, Laura Gustafson, Tete Xiao, Spencer Whitehead, Alexander C Berg, Wan-Yen Lo, et al. Segment anything. In *Proceedings of the IEEE/CVF International Conference on Computer Vision*, pages 4015–4026, 2023.
- [10] Jonas Kulhanek, Songyou Peng, Zuzana Kukelova, Marc Pollefeys, and Torsten Sattler. Wildgaussians: 3d gaussian splatting in the wild. *arXiv preprint arXiv:2407.08447*, 2024.
- [11] Jaewon Lee, Injae Kim, Hwan Heo, and Hyunwoo J Kim. Semantic-aware occlusion filtering neural radiance fields in the wild. *arXiv preprint arXiv:2303.03966*, 2023.
- [12] Yiqing Liang, Numair Khan, Zhengqin Li, Thu Nguyen-Phuoc, Douglas Lanman, James Tompkin, and Lei Xiao. Gaufré: Gaussian deformation fields for real-time dynamic novel view synthesis. *arXiv preprint arXiv:2312.11458*, 2023.
- [13] Tsung-Yi Lin, Michael Maire, Serge Belongie, James Hays, Pietro Perona, Deva Ramanan, Piotr Dollár, and C Lawrence Zitnick. Microsoft coco: Common objects in context. In *Computer vision—ECCV 2014: 13th European conference, zurich, Switzerland, September 6–12, 2014, proceedings, part v 13*, pages 740–755. Springer, 2014.

- [14] Andrew Liu, Richard Tucker, Varun Jampani, Ameesh Makadia, Noah Snavely, and Angjoo Kanazawa. Infinite nature: Perpetual view generation of natural scenes from a single image. In *Proceedings of the IEEE/CVF International Conference on Computer Vision*, pages 14458–14467, 2021.
- [15] Fangfu Liu, Wenqiang Sun, Hanyang Wang, Yikai Wang, Haowen Sun, Junliang Ye, Jun Zhang, and Yueqi Duan. Reconx: Reconstruct any scene from sparse views with video diffusion model. *arXiv preprint arXiv:2408.16767*, 2024.
- [16] Tianqi Liu, Guangcong Wang, Shoukang Hu, Liao Shen, Xinyi Ye, Yuhang Zang, Zhiguo Cao, Wei Li, and Ziwei Liu. Mvsgaussian: Fast generalizable gaussian splatting reconstruction from multi-view stereo. In *European Conference on Computer Vision*, pages 37–53. Springer, 2025.
- [17] Yuan Liu, Sida Peng, Lingjie Liu, Qianqian Wang, Peng Wang, Christian Theobalt, Xiaowei Zhou, and Wenping Wang. Neural rays for occlusion-aware image-based rendering. In *Proceedings of the IEEE/CVF Conference on Computer Vision and Pattern Recognition*, pages 7824–7833, 2022.
- [18] Ricardo Martin-Brualla, Noha Radwan, Mehdi SM Sajjadi, Jonathan T Barron, Alexey Dosovitskiy, and Daniel Duckworth. Nerf in the wild: Neural radiance fields for unconstrained photo collections. In *Proceedings of the IEEE/CVF conference on computer vision and pattern recognition*, pages 7210–7219, 2021.
- [19] Ben Mildenhall, Pratul P Srinivasan, Matthew Tancik, Jonathan T Barron, Ravi Ramamoorthi, and Ren Ng. Nerf: Representing scenes as neural radiance fields for view synthesis. *Communications of the ACM*, 65(1):99–106, 2021.
- [20] Thang-Anh-Quan Nguyen, Luis Roldão, Nathan Piasco, Moussab Bennehar, and Dzmityr Tsishkou. Rodus: Robust decomposition of static and dynamic elements in urban scenes. *arXiv preprint arXiv:2403.09419*, 2024.
- [21] Takashi Otonari, Satoshi Ikehata, and Kiyoharu Aizawa. Entity-nerf: Detecting and removing moving entities in urban scenes. In *Proceedings of the IEEE/CVF Conference on Computer Vision and Pattern Recognition*, pages 20892–20901, 2024.
- [22] Lu Qi, Jason Kuen, Weidong Guo, Tiancheng Shen, Jiuxiang Gu, Jiaya Jia, Zhe Lin, and Ming-Hsuan Yang. High-quality entity segmentation. *arXiv preprint arXiv:2211.05776*, 2022.
- [23] Weining Ren, Zihan Zhu, Boyang Sun, Jiaqi Chen, Marc Pollefeys, and Songyou Peng. Nerf on-the-go: Exploiting uncertainty for distractor-free nerfs in the wild. In *Proceedings of the IEEE/CVF Conference on Computer Vision and Pattern Recognition*, pages 8931–8940, 2024.
- [24] Sara Sabour, Lily Goli, George Kopanas, Mark Matthews, Dmitry Lagun, Leonidas Guibas, Alec Jacobson, David J Fleet, and Andrea Tagliasacchi. Spotlessplats: Ignoring distractors in 3d gaussian splatting. *arXiv preprint arXiv:2406.20055*, 2024.
- [25] Sara Sabour, Suhani Vora, Daniel Duckworth, Ivan Krasin, David J Fleet, and Andrea Tagliasacchi. Robustnerf: Ignoring distractors with robust losses. In *Proceedings of the IEEE/CVF Conference on Computer Vision and Pattern Recognition*, pages 20626–20636, 2023.
- [26] Matthew Tancik, Ethan Weber, Evonne Ng, Ruilong Li, Brent Yi, Terrance Wang, Alexander Kristoffersen, Jake Austin, Kamyar Salahi, Abhik Ahuja, et al. Nerfstudio: A modular framework for neural radiance field development. In *ACM SIGGRAPH 2023 Conference Proceedings*, pages 1–12, 2023.
- [27] Paul Ungermann, Armin Effenhofer, Matthias Nießner, and Barbara Roessle. Robust 3d gaussian splatting for novel view synthesis in presence of distractors. *arXiv preprint arXiv:2408.11697*, 2024.
- [28] Peihao Wang, Xuxi Chen, Tianlong Chen, Subhashini Venugopalan, Zhangyang Wang, et al. Is attention all that nerf needs? *arXiv preprint arXiv:2207.13298*, 2022.

- [29] Qianqian Wang, Zhicheng Wang, Kyle Genova, Pratul P Srinivasan, Howard Zhou, Jonathan T Barron, Ricardo Martin-Brualla, Noah Snavely, and Thomas Funkhouser. Ibrnet: Learning multi-view image-based rendering. In *Proceedings of the IEEE/CVF Conference on Computer Vision and Pattern Recognition*, pages 4690–4699, 2021.
- [30] Jiacong Xu, Yiqun Mei, and Vishal M Patel. Wild-gs: Real-time novel view synthesis from unconstrained photo collections. *arXiv preprint arXiv:2406.10373*, 2024.
- [31] Chuanrui Zhang, Yingshuang Zou, Zhuoling Li, Minmin Yi, and Haoqian Wang. Transplat: Generalizable 3d gaussian splatting from sparse multi-view images with transformers. *arXiv preprint arXiv:2408.13770*, 2024.
- [32] Dongbin Zhang, Chuming Wang, Weitao Wang, Peihao Li, Minghan Qin, and Haoqian Wang. Gaussian in the wild: 3d gaussian splatting for unconstrained image collections. *arXiv preprint arXiv:2403.15704*, 2024.
- [33] Tinghui Zhou, Richard Tucker, John Flynn, Graham Fyffe, and Noah Snavely. Stereo magnification: Learning view synthesis using multiplane images. *arXiv preprint arXiv:1805.09817*, 2018.